Chemical Vapor Deposition 19 (10-12) (2013) 338-346

Surface Immobilized Gold Nanoparticles by Organometallic Chemical Vapor Deposition on Amine Terminated Glass Surfaces

Erden Ertorer[a,b], Jessica C. Avery[c], Laura C. Pavelka[c] and Silvia Mittler[b*]

[a]Biomedical Engineering Program, Faculty of Engineering, University of Western Ontario (Western University), London, ON, Canada

[b]Department of Physics and Astronomy, University of Western Ontario (Western University), London, ON, Canada

[c]Department of Chemistry, University of Western Ontario (Western University), London ON, Canada

(Corresponding author: smittler@uwo.ca)

Abstract

We describe the growth of surface immobilized gold nanoparticles with organometallic chemical vapour deposition (OMCVD) on amine terminated surfaces, utilizing (trimethylphospine)methylgold ($(CH_3)_3PAuCH_3$) precursor. Samples fabricated using different deposition times were characterized by UV-Vis spectroscopy and scanning electron microscopy. Particle stability on the samples was tested by washing and rinsing treatments with various organic solvents. A biotin-streptavidin scheme was applied to demonstrate the biosensing capabilities of the samples. The size, interparticle distance, and shape of the gold nanoparticles demonstrated that OMCVD is a simple, economic, and fast way to fabricate surface bonded and stable gold nanoparticles. The plasmonic properties, the stability of the particles and the biotin-streptavidin test showed that these OMCVD-grown gold nanoparticles are suitable for reproducible, low noise and highly sensitive biosensing applications.

Key Words: gold nanoparticles, OMCVD, chemical vapour deposition, silanization, biosensor applications

* corresponding author: fax: 1 519 661 2033, e-mail: smittler@uwo.ca

1. Introduction

Gold nanoparticles (AuNPs) serve in a variety of scientific, medical and engineering applications, for example acting as biosensors,[1]–[3] catalysts for nanowire or nanotube growth,[4]–[7] and photovoltaics.[8]–[10] In addition to their plasmonic properties,[11]–[14] the chemical properties of gold make them highly suitable for label free, extremely sensitive biosensor applications.[15][16]

Although colloidal gold is easy to synthesize, it has many disadvantages over substrate immobilized AuNPs. Besides the potential environmental and health impact of solution-based "free" AuNPs, they require a stabilizing agent to prevent aggregation. Typically a citrate layer or a polymer coating is used to create a core-shell structure.[17] The introduction of this stabilization agent surface chemistry makes further functionalization for the application complicated. Substrate immobilized colloidal gold nanoparticle (AuNP) samples inherit the same problem. In addition, due to its liquid nature, colloidal gold requires additional handling considerations for lab-on-a-chip applications. Moreover, the 3D form of colloidal gold requires a higher volume of sample for sensing applications in comparison to "2D" surface immobilized particles.

Conventional substrate immobilized gold nanoparticle (AuNP) fabrication methods such as focused ion beam or electron beam lithography require costly setups and also suffer from low speed and small area of coverage. For prototype purposes, these drawbacks can be neglected. However, for industrial or clinical applications mass production is necessary; cost-effective, simple, and fast methods are required.

Chemical vapor deposition (CVD) is a well-studied method to produce thin films on substrate surfaces[18][19][20] mainly used in microelectronic technology.[21] In the last two decades nanotechnology started to take advantage of various forms of CVD in many different fabrication purposes. Although nanotubes[22][23] and nanowires[24][25] are the most known nanostructures produced by CVD, a variety of other structures has been reported, such as AuNPs,[26][27] AuNP/semiconductor and AuNP/titania

composites,[28] AuNP/transition metal composites,[29] SiO_2 sandwitched AuNP arrays,[30] AuNP doped vanadium dioxide thin films,[31] and titanium dioxide/tin dioxide nanocomposites.[32]

Organometallic precursors form metallic thin films on substrate surfaces.[18][33][34] Under certain conditions, film growth follows an island formation scheme, which is also known as Volmer–Weber growth[36]. Interrupting the procedure before forming thin films yields metallic nanoparticles. [19][27][34][35] In terms of wetting conditions, the Volmer–Weber growth mechanism can be expressed mathematically by the Young-Dupre equation [36]:

$$\gamma_{SV} = \gamma_{CS} + \gamma_{CV} cos\theta \qquad [1]$$

In this equation γ_{SV} is substrate-vacuum surface energy, γ_{CS} the substrate-film interface energy and γ_{CV} the film-vacuum surface energy (Figure 1).

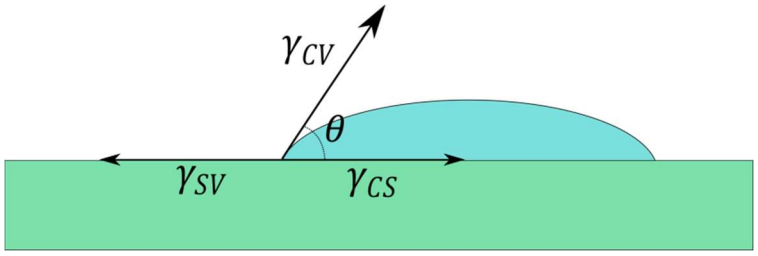

Figure 1- Wetting angle and surface energies in Volmer-Weber growth

For values of θ higher than 0° attractive forces between the two deposited metal atoms are higher than the forces between the substrate and the deposited metal atom. Therefore a stable film structure is not favorable but island growth occurs.[36]

CVD is a surface chemistry selective process, meaning the substrate surface can be functionalized, creating areas with and without film growth.[33][34][37][38] The desired surface functionalization to create nucleation sites can be achieved for example, by a self-assembly process; dithiols are used on metallic

surfaces and silanes on oxidized surfaces to form self-assembled monolayers (SAMs).[39] The stability of the AuNPs grown by OMCVD strongly depends on the quality of the self-assembled monolayer (SAM). The localized surface plasmon resonance (LSPR) frequency of AuNPs lies in the visible part of the electromagnetic spectrum; therefore, the substrate should be transparent for transmission-based plasmonic sensors applications. Although glass substrates are high quality and widely used for similar purposes, our studies show that functionalization of the glass surface by employing wet silane chemistry is especially challenging.[40] The self-assembly process is very sensitive to experimental conditions, including temperature and humidity, which decreases batch-to-batch reproducibility and stability of the AuNPs on the surface.[41]–[44] When flushing is required for a biosensor application in a liquid handling system, the immobilization stability of the particles, the ability to not being moved by the liquid, is especially crucial. Poor quality of the SAM causes particles to be physisorbed on the surface, missing the chemical bonds to the substrate. These physisorbed particles can then be moved by the sensor solution, and cause undesired optical effects in the biosensor application. Typically, NP aggregation on the surface occurs, creating false signals or, due to detachment and loss of particles, a decrease in signal and/or in the signal-to-noise ratio emerges.[40]

In this study, we introduced the growth of stable AuNPs on amine functionalized BK7 glass surfaces via OMCVD using (trimethylphospine)methylgold ($(CH_3)_3P]AuCH_3$) precursor. Amine groups are known for their strong affinity to gold.[17][45] Several studies were reported immobilizing colloidal AuNPs on aminosilane functionalized surfaces.[25][46]–[48] Hexamethyldisilazane (HMDS) silanization is a standard process in lithography to enhance photoresist adhesion.[49] In order to create nucleation sites for growth of AuNPs by OMCVD, surface functionalization of the substrate was achieved by vapor deposition of HMDS in a totally environmentally controlled vapor deposition oven, instead of wet chemistry in a glove box. We systematically varied the OMCVD time to investigate the time dependence of the size and interparticle distance properties of these randomly positioned AuNPs. The

samples fabricated with different OMCVD times were characterized by UV-Vis absorption spectroscopy and scanning electron microscopy. Correlations between growth time, size, interparticle distance, and UV-Vis absorption maxima were established. Stability tests were performed by washing and rinsing cycles using various organic solvents to simulate liquid handling systems in sensor applications. The biosensing capabilities of the stable OMCVD-grown AuNP samples were tested by implementing the well-known biotin-streptavidin system[50].

2. Results

Figure 2a shows absorption spectra of eight individual samples grown for 15 min in the OMCVD reactor. The maximum of the absorption spectrum corresponds to the localized surface plasmon resonance (LSPR) peak. The averaged absorption spectra for the eight samples in each batch for the various OMCVD times are depicted in Figure 2b. Figure 2c shows the position of the absorption peak maximum with increasing growth time. With increasing OMCVD time, the LSPR peak shifted to the red with increased standard deviation.

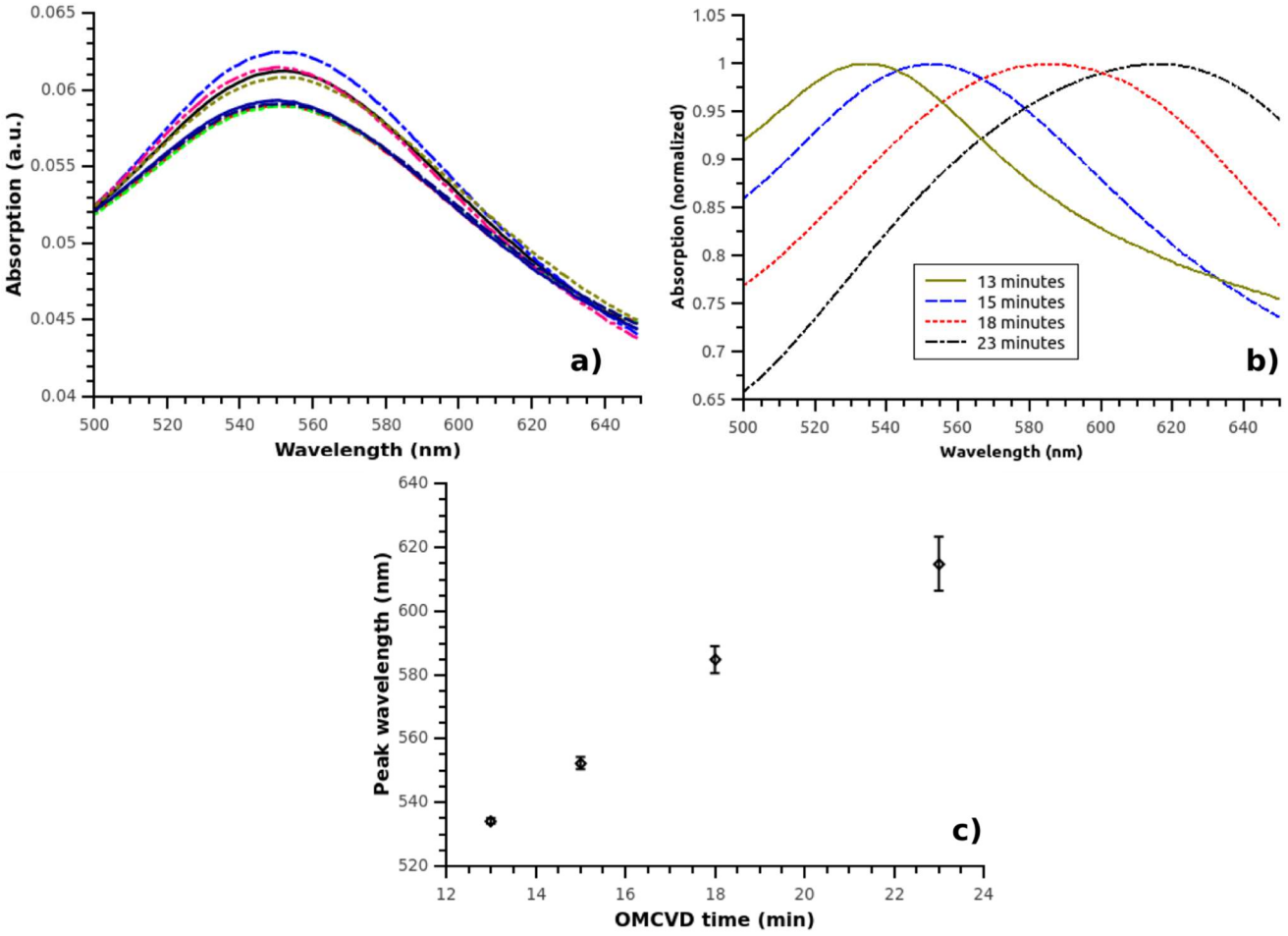

Figure 2 - Spectral properties of AuNPs fabricated by OMCVD: a) absorption spectra of eight samples from a single batch with an OMCVD growth time of 15 min, b) averaged absorption spectra for different OMCVD times averaged over all samples in the batches, c) spectral LSPR position as a function of OMCVD time

Since differences between absorption spectra of samples within the same batch were negligible compared with differences between samples from different batches with increasing OMCVD times (Fig. 2c), one sample from each batch was selected and electron microscopy images were taken of eight locations uniformly distributed on these samples (Fig. 3a, inset). Figure 3a is an SEM image with 20,000 x magnification showing the uniformity at a wide area. A 100,000 x magnification allowed observation of the shapes of the individual nanoparticles (Fig. 3b). For lower OMCVD times, AuNPs were round (Fig. 3b, bottom). Increasing the OMCVD time yielded nanoparticles with corners, or even

star shapes exhibiting clear crystalline facets (Fig. 3b, top) which indicates the crystalline structure of OMCVD grown AuNPs on SH terminations as previously reported.[27]

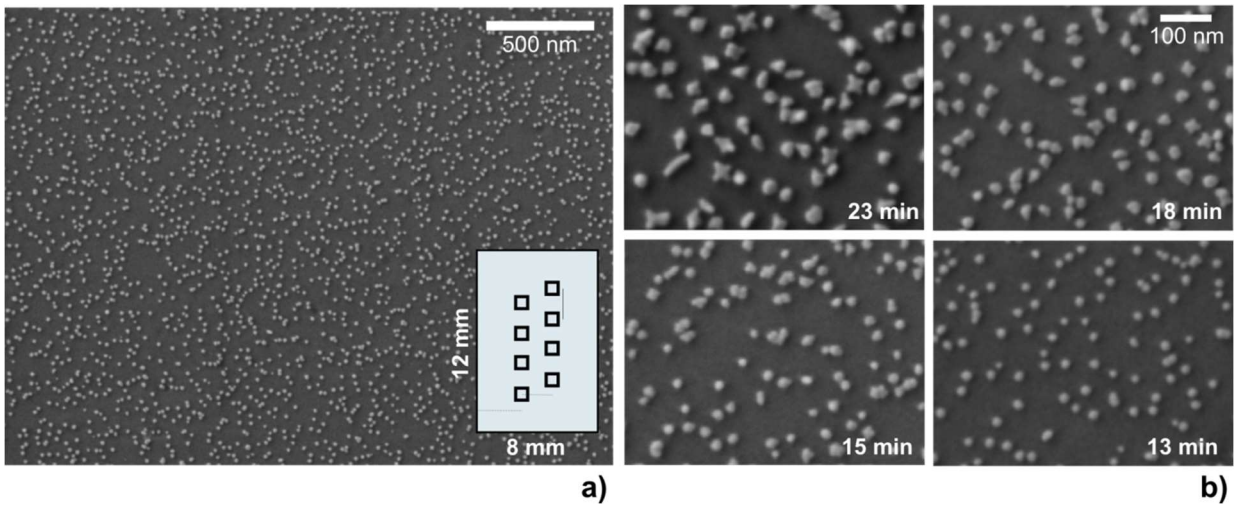

Figure 3 - Scanning electron micrographs of AuNPs grown on –NH functionalities: a) view at large scale (t_{OMCVD}= 15 min). The inset shows the sample geometry and the positions where the eight higher resolution images were taken. b) High magnification of samples fabricated with OMCVD times from 13-23 min.

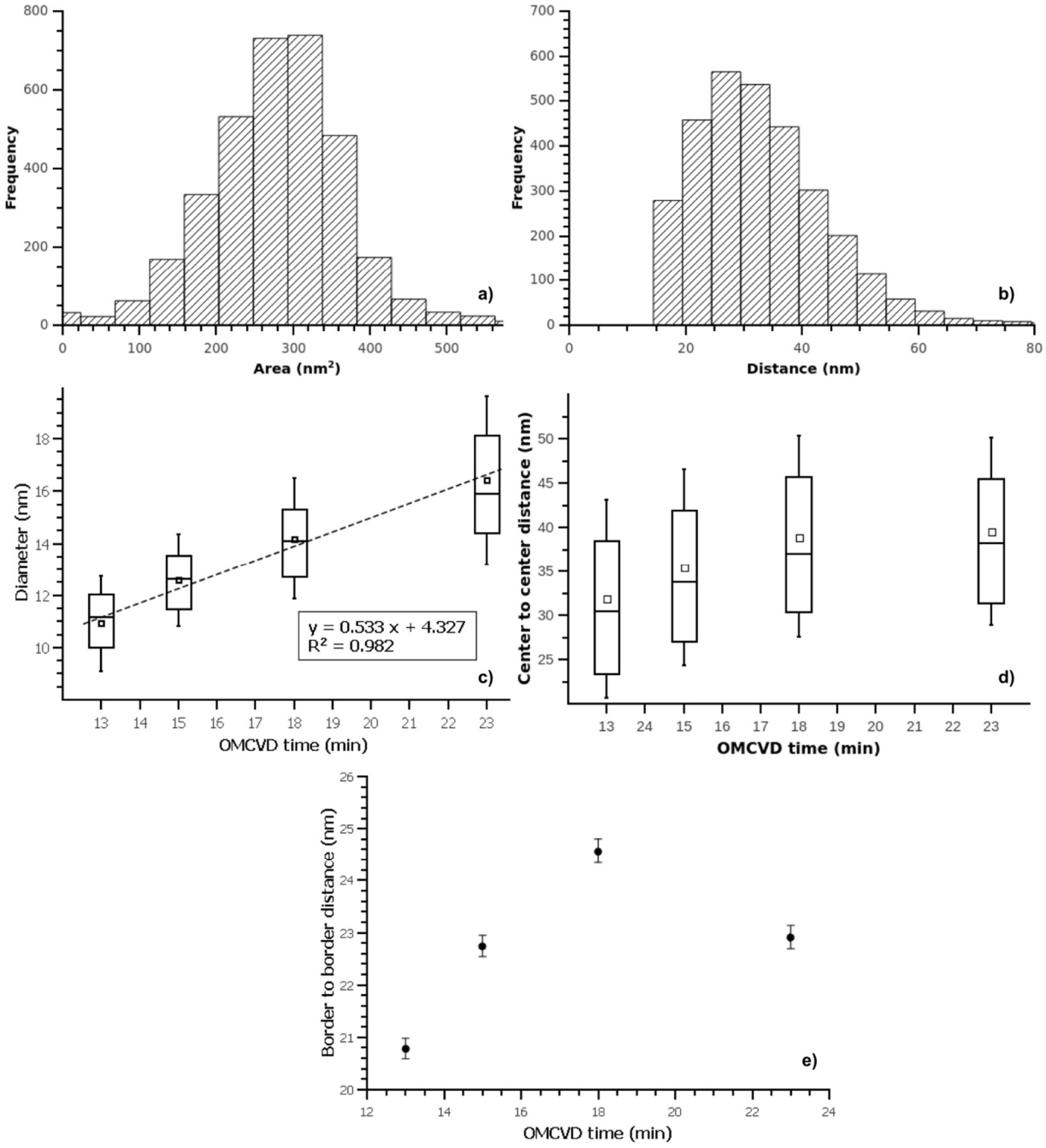

Figure 4 - Size and distance distribution of AuNPs: a) area histogram of 13 min OMCVD sample, b) center-to-center distance histogram of 15 min OMCVD sample, c) box plot of calculated diameters of the samples with various OMCVD time (assuming round objects in all cases), d) box plot of center-to-center distance with OMCVD time, e) calculated border-to-border distance as a function of OMCVD time with standard error. For both diameter and distance measurements, the error bars show the standard deviation, the boxes show the 25% to 75% intervals of the data, and the small square dots show the mean values.

The size and distance between individual AuNPs were analyzed in the scanning electron micrographs. Figure 4a is a representative example showing the area distribution of the 13 min OMCVD sample as measured and analysed by SEM. Figure 4b shows the distribution of the center-to-center interparticle distance for the 15 min OMCVD sample. For the other batches with increased OMCVD time, the shape of the histograms remained the same, although the particle size shifted to higher values and larger variation in size was observed.

Low OMCVD times led to growth of small particles, increasing time yielded larger particles with less uniform size distributions. Figure 4c shows the diameter distribution of the particles based on a calculation of the diameter from the area. Although not all AuNPs obtained by growth for 18 min or 23 min were round, their areas were approximated as circles to give a clear sense of size when the data were converted to diameters. The calculated average diameter increased from ~11 nm to ~17 nm in a linear fashion by increasing the growth time from 13 to 23 min, implying a growth kinetic constant of roughly 0.5 nm/min.

The average center-to-center distance between the AuNPs increased with reaction time and reached a plateau (Fig. 4d). As depicted in Figure 4e, the mean border-to-border distance, calculated from the diameter and interparticle distance distributions, increased up to 18 min and then decreased slightly.

It is critical to ensure the stability of the particles used in biosensor applications. The absorption spectra of our samples remained unchanged within the error range of the spectrometer after applying all rinsing cycles in the stability tests. Changes in the absorption maximum were lower than 0.1 nm which is the measurement error of the experiment. AuNP formation is also observed for cleaned glass samples without HMDS functionalization. However, the LSPR vanished after the stability tests indicating that the AuNPs did not stay on the surface. They were washed off, indicating a poor attachment to the surface. AuNP formation and deposition can be completely avoided by functionalizing the surface with $–CH_3$ (see Experimental: surface functionalization of the OMCVD reactor).

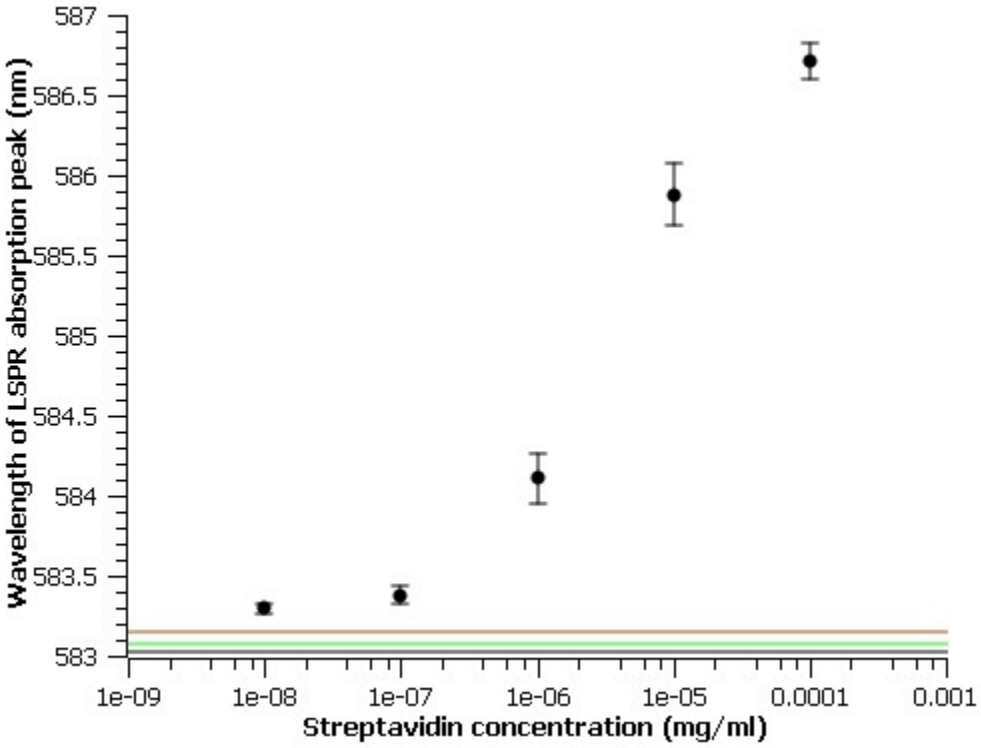

Figure 5 - Streptavidin concentration response of OMCVD AuNP-based sensor. The black line represents the base line, the yellow line the detection uncertainty, and the red line the base line plus three times the detection uncertainty.

Figure 5 shows the sensor response of the high affinity system biotin-streptavidin. The biotin recognition site is immobilized on the AuNPs and the streptavidin is detected due to its binding to the biotin moieties[50]. The dipolar LSPR spectral position versus increasing streptavidin concentration was investigated on samples with a growth time of 15 minutes giving ~13 nm of mean particle diameter and 23 nm of average border to border distance. Between 10 ng/ml to 100 µg/ml concentration range the limit of detection was calculated by the 3σ method[51] and was found to be better than 10 ng/ml (~200 pM).

3. Discussion

The high affinity of gold to amine has been used in multiple cases for the immobilization of gold colloids, however the precise chemical mechanism has not been discussed.[17][25][45]-[48] The –NH terminated surface investigated here obviously serves as a growth surface for OMCVD of AuNPs; nucleation and growth happens. It is not within the scope of this work to determine the exact reaction mechanism of the Au-precursor to the available –NH groups, however we assume a favourable interaction between the lone electron pair of the nitrogen on the sample surface and the Au(I) in the precursor. Gold exists in various oxidation states. Au(I), for example as present in the implemented precursor, forms numerous complexes of which many are stable, but also easily undergo ligand exchange reactions.[52] The $(CH_3)_3P]AuCH_3$ precursor is a donor-acceptor complex[53], potentially involving Lewis acid (LA)- Lewis base (LB) interaction. We propose for the first growth step a surface-ligand-exchange reaction, where the phosphorous group of the precursor, $-P-(CH_3)_3$ (the LB of the precursor) is displaced by the nitrogen group –NH (the new LB) on the surface. With this first step, the LB $Au-CH_3$ is immobilized at the surface via the Au(I) whereas the phosphorous group is released into the gas phase. The binding constants from Au(I) to the $-P-(CH_3)_3$ was found to be 242.42 kJ/mol experimental and 250.37 kJ/mol theoretical, respectively[53]; whereas the binding energy of Au^+-NH_3 was found to be 265.86 kJ/mol[54], larger in comparison to the phosphorous. The binding energy of Au(1)-NH may be even larger.

In a second step, due to the high gold-gold affinity, the Au of a second precursor molecule may bind to the immobilized gold species. When the oxidation state of the Au nucleus changes into a Au(0) state cannot be demined without additional experiments.

Due to the LSPR phenomenon, the size, interparticle distance and shape of the AuNPs determine their absorption spectrum.[11]–[14] Therefore, UV-Vis absorption spectroscopy provides an easy and economical way to characterize such samples. The LSPR peak shifted to the red with increasing OMCVD time, indicating that the particle size increased, the interparticle distance decreased, and/or

the particle shape changed from a round to a more angular shape.[11][12] The increase in the observed standard deviation indicated that increasing the growth time increased the inhomogeneity of the samples.

For all samples and all batches, the relative standard deviation in the particle number observed in the images for the eight locations was less than 10%, which indicated homogeneity of the particle distribution along the surface. Figure 3a is an SEM image with 20,000 x magnification showing the uniformity at a wide area. A 100,000 x magnification allowed observation of the shapes of the individual nanoparticles (Figure 3b). For shorter OMCVD times, AuNPs were round (Fig. 3b, bottom). Increasing the OMCVD time yielded nanoparticles with corners, or even star shapes (Fig. 3b, top). Round particles are useful for transmission-based plasmonic sensor applications and nanowire growth.[7][55] Particles with corners are suitable for surface enhanced Raman spectroscopy (SERS) applications, due to hot spot formation around the edges.[56]–[60]

The size and distance between the AuNPs are important parameters for plasmonic sensors, and the LSPR properties of the particles strongly depend on them. Narrow particle size distribution is usually desired for biosensor applications. If the LSPR band increases in width, errors in determining the absorption peak spectral position increase which decreases the limit of detection.[61] Although OMCVD is a statistical process, the box plot in Figure 4c shows a narrow size distribution comparable with colloidal gold produced by the citrate reduction method.[62] On the other hand, limit of detection calculations with the biotin-streptavidin platform showed that size distribution allows biosensor applications.

Increase in the average center-to-center distance between the AuNPs with reaction time (Fig. 4d) showed that for the shorter times, AuNPs were individually well separated. With increasing time, close particles merged, forming a single larger particle. This merging increased the average interparticle distance until most particles were large and again well separated. The shape of the border-to-border

distance curve is a result of close-particle-merging and increase in the particle size by time. After 18 min, most of the close particles had merged (Fig. 4d), and therefore, the center-to-center distance did not increase anymore. However, the diameter of the nanoparticles kept increasing, which decreased the border-to-border distance after 18 min (Fig. 4e), creating hot spots for surface enhanced Raman spectroscopy[56][57] and enabling optical cross-talk as a sensing mechanism for transmission-based sensors.[3][26][37] Such a close spacing of ~20 nm between the particles has not been achieved by conventional fabrication methods such as electron beam lithography or focused ion beam lithography.

Fabrication of AuNPs with a precise size is possible by adjusting the OMCVD time. However, it should be noted that increasing OMCVD time will yield less uniformity in shape, size, and interparticle distance. Higher reaction times will lead to connected AuNPs, creating islands and eventually yielding a thin film of gold.[19]

For a quick and economic characterization process, it would be valuable to learn about the size distribution of the AuNPs by UV-Vis absorption spectra. Figure 6 shows the relationship between the spectral peak position of the LSPR and the diameter of the AuNPs. The spectral position of the LSPR showed a linear relationship to the average diameter.

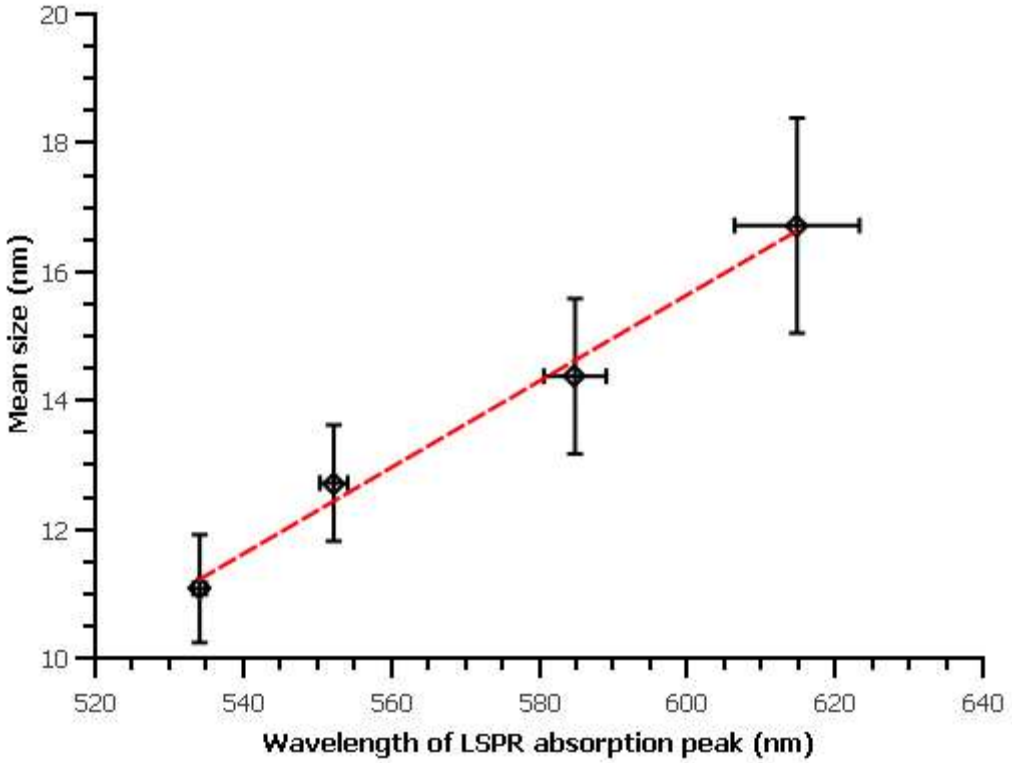

Figure 6 - Relationship between wavelength of the LSPR absorption maximum and the average particle diameter of the AuNPs.

Amine functionalized samples with AuNPs were stable against washing/rinsing experiments simulating liquid handling conditions. This showed that the particles are chemically bonded to the surface. Absence or poor quality of the HMDS SAM on the substrate caused loosely attached AuNPs; the particles "float", aggregate, or move away from the surface.[40] Losing of particles decreases the strength of the LSPR of the sample and decreases the signal-to-noise ratio in the absorption spectrum. Aggregation of the particles causes cross-talk, which appears as a shoulder in the absorption spectrum or widens the LSPR peak, leading to larger errors and higher noise if the dipolar LSPR peak is used to determine the sensor signal.

LSPR of AuNPs is highly sensitive to changes in the refractive index of the surrounding environment, which is the phenomenon behind the plasmonic sensors. Biotinilated-thiol is the linker molecule

between the AuNPs and streptavidin.[50] As the concentration of the protein streptavidin increases, the surface coverage of streptavidin on the biotin labels on the nanoparticles increases appearing as a red shift in the LSPR absorption maximum. The limit of detection is 10 ng/ml (~200 pM) being in the same order of magnitude than other nanoparticle surface plasmon resonance sensors reported.[2][63][64] This proof of principle experiment can easily be modified by using appropriate linker chemistry to detect any important biomolecule. The dependence on the linker chemistry, especially the dependency on the particular binding constant, and the AuNP size must be optimized for each individual sensor to achieve the highest possible sensitivity. To employ the optical cross-talk in a sensor scheme additionally the AuNP interparticle distance must be optimized.[65]

4. Conclusion

We have introduced a new, simple and inexpensive approach for fabricating highly stable AuNPs via OMCVD on amine functionalized glass surfaces. Increasing the OMCVD time yielded larger particle sizes and closer border-to-border spacing. Round particles were transformed to angular particles and their size became less uniform with increased deposition times. Increasing size, decreasing spacing and a change into angular shapes caused a red shift in the LSPR of the AuNPs. Therefore, we were able to establish a relationship between the AuNP attributes and their absorption spectrum. Vapor phase deposition of HMDS in an oven provided reproducible and high quality amine functionalization. Washing and rinsing cycles with various solvents to simulate the liquid handling conditions of biosensor applications did not cause a change in the absorption spectra of the samples, indicating that the AuNPs were stably held in position on the substrate. Biotin-streptavidin recognition experiments showed the biomolecule sensing capabilities of the samples. AuNPs fabricated by OMCVD could be used for biosensor applications; however, the effect of size, shape and interparticle distance on fundamental sensor parameters such as limit of detection and sensitivity must be investigated and fine-tuned for each individual linker-chemistry applied.

The effect of various temperatures and pressures used in the OMCVD process in terms of the size, shape and interparticle distance of the resulting particles needs further investigation. It is expected that a decrease in reaction temperature will slow the growth rate, so that fine tuning, especially for smaller particles, will become feasible. Control of interparticle spacing and improved uniformity may also be achievable. The interparticle distance could be adjusted independently using various techniques for sensor tunability, such as manipulating the binding sites with FIB[63][64] or using binary mixtures of HMDS and OTS.[66]-[68]

These stable OMCVD AuNPs can also be used where substrate immobilized bare AuNPs are required, e.g. for the growth of nanowires and fabricating photovoltaic devices. Depending on the application, different substrates can be used as long as amine functions can be bonded to the surface. This process itself does not involve any wet chemistry nor ion beam technology; it is therefore advantageous for 3D samples with a complicated surface geometry, and can direly be applied in lab-on-a-chip technology.

5 Experimental

5.1. Fabrication of AuNP samples

All chemicals were used without further purification. BK7 (Hellma, Germany) glass slides (8 x 12 mm) were immersed in Nano-Strip solution (Cyantek Inc., CA, USA) at 60°C for 20 min to remove possible contaminants. Substrates were then rinsed with abundant amounts of Milli-Q water (MilliPore, MA, USA), dried with nitrogen, and placed in an STS Reactive Ion Etch system (STS Surface Technology Systems, Newport, UK) in an oxygen plasma at 80 W for 20 min to oxidize the substrate surface, creating –OH functionalities (Fig. 9a). The hydrophilic nature of the samples was confirmed by contact angle measurements ($\theta < 2°$) (Reme-Hart Model 200 Ganiometer, Reme-Hart Co. NJ, USA). For surface functionalization with –NH groups, silanization of the substrates with 100% HMDS (Fig. 7a) (Transene Inc., MA, USA) in a YES-3TA HMDS vacuum oven (Yield Engineering, CA, USA) was

carried out. The contact angle θ, measured as 68.9° ± 0.6°, confirmed the surface modification.

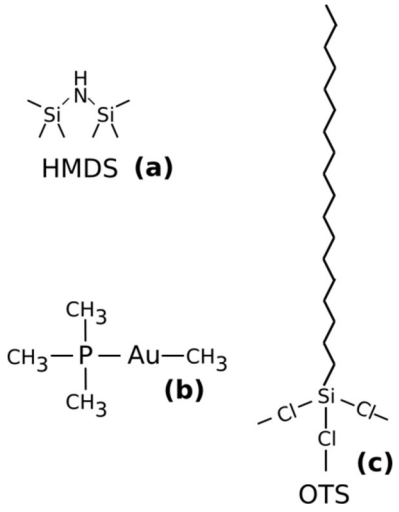

Figure 7 - Structure formula of compounds implemented in AuNP sample fabrication and to yield an inert glass reactor: a) hexamethyldisilazane (HMDS), b) the organometallic gold precursor trimethylphosphinegoldmethyl ($[(CH_3)_3P]AuCH_3$), and c) octadecyltrichlorosilane (OTS)

The inner surface of a glass reactor (Figure 8) was functionalized wet chemically with octadecyltrichlorosilane (OTS) (Fig. 7c), which forms a non-growth surface. This SAM avoids gold deposition on the inner walls of the reactor.[38] This procedure increases the efficiency of the AuNP growth process by avoiding unnecessary precursor consumption. First, the OMCVD glass reactor was filled with freshly prepared piranha solution (1:3 v:v H_2O_2:H_2SO_4). It was given two hours to oxidize the inner surface (creating –OH functionalities). The reactor was then rinsed with copious amounts of Milli-Q water, dried with nitrogen, and placed in a vacuum oven at 95°C for 20 min to remove any moisture from its surface. A 1:500 v:v mixture of OTS (97%, Sigma, Ontario, Canada) in toluene (Caledon Lab. Inc, Georgetown, ON, Canada) was freshly prepared. The OMCVD reactor was filled with the OTS solution overnight under an argon environment in a glove box. After SAM formation the reactor was rinsed with toluene and placed in a vacuum oven at 95°C for 20 min to form silane bonds and expel toluene from the reactor surface.

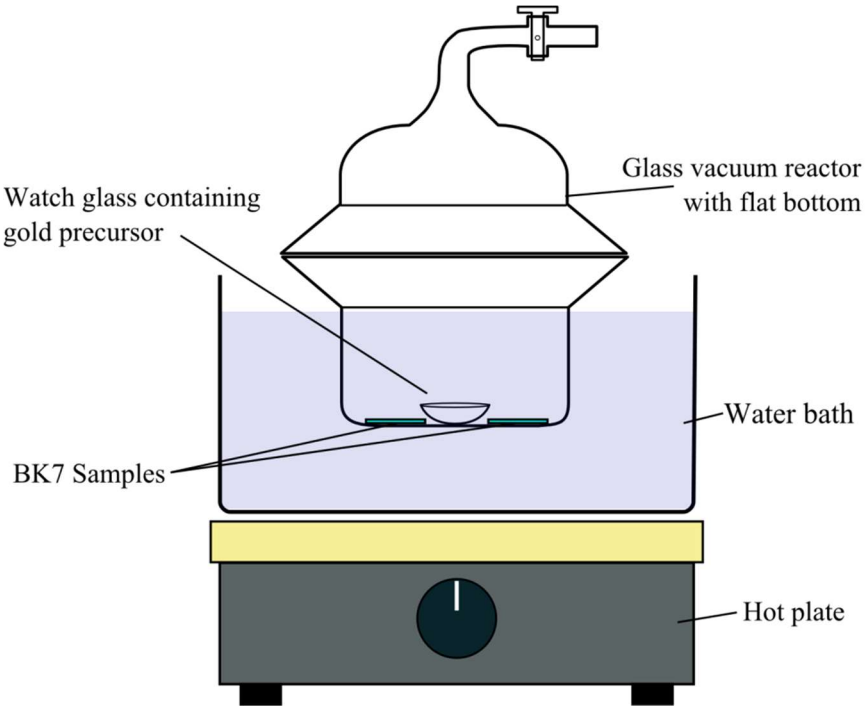

Figure 8 - Illustration of the OMCVD setup

Amine functionalized substrates were placed on the reactor's flat glass bottom as well as a small watch glass containing 20 mg of the organometallic gold precursor trimethylphosphinegoldmethyl ($[(CH_3)_3P]AuCH_3$) (Fig. 6b). The synthesis of the precursor is described elsewhere.[69] Uniform thermal contact between the reactor bottom and the samples is guaranteed by the flat-bottom reactor. Even temperature distribution along the surface of the substrate yields a uniform nucleation site density, which provides homogenous growth over the surface. The reactor was pumped down to >5 Pa and filled with argon for three cycles to ensure an inert atmosphere inside the reactor. During the last cycle, the internal pressure was set to 5 Pa. The reactor was placed in a water bath preheated to 65°C for 13, 15, 18 and 23 min. After the deposition period, the reactor was immediately vented and the samples with the grown AuNPs were removed.

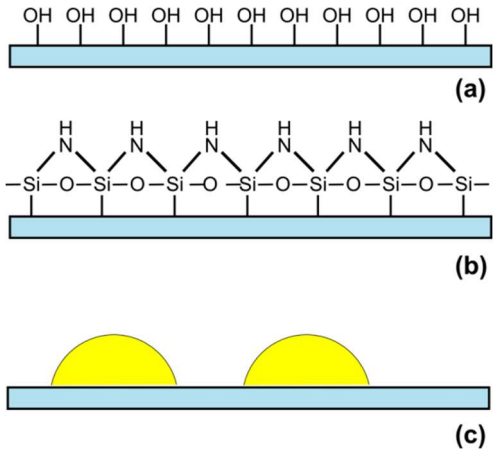

Figure 9 - Surface modification **s**cheme: a) substrate with oxidized surface after piranha treatment; b) silane network after HMDS functionalization; c) AuNPs on the substrate without chemistry details of the HMDS layer (not to scale)

5.2. Characterization

UV-Vis absorption spectra were obtained using a LAMBDA 850 UV-Vis recording spectrophotometer (PerkinElmer, Ca, USA). The absorption spectrum of a blank BK7 glass was used as a reference.

Scanning electron micrographs were acquired by a Leo 1530 scanning electron microscope (LEO Electron Microscope, Zeiss, Germany). Prior to imaging, samples were coated with 1 nm of osmium to make them conductive. ImageJ[70] software was used for processing the images. The area and two-dimensional center of mass data were extracted from the images to calculate the distribution of the center-to-center interparticle distance using a nearest neighbour algorithm.

5.3. Stability tests

Two samples from each batch corresponding to different OMCVD growth times were rinsed with anhydrous ethanol several times to remove physisorbed particles, and then dried. After acquiring a UV-Vis absorption spectrum, the samples were immersed and rinsed repeatedly with methanol, isopropanol, and dichloromethane and then immersed in Phosphate Buffered Saline (PBS) buffer and rinsed with Milli-Q water and isopropanol.

5.4. Biosensing

Samples were immersed in 0.45 mM 11-mercaptoundecanol (Sigma-Aldrich, Ontario, Canada), an OH terminated thiol, and 0.05 mM biotinylated thiol (NanoScience Chemicals, Phoenix, AZ, USA) in anhydrous ethanol solution for two hours to form a SAM with biotin moieties. Repeated washing with ethanol was followed by drying the sample with nitrogen. The samples were immersed first in PBS buffer and then in increasing concentrations of streptavidin in PBS buffer.

Acknowledgements

The authors thank the Western Nanofabrication Facility for their help in the fabrication process and with scanning electron microscopy. The authors also thank Kim Baines for hosting the precursor synthesis in her lab. Hao Jiang, Max Port, Tayirjan Isimjan, Joe Gilroy and Chitra Rangan are acknowledged for their helpful discussions. The NSERC BiopSys Strategic Network is thanked for financial contributions. CFI and the Ontario Innovation Trust are thanked for funding equipment. E.E. thanks the Ontario Graduate Scholarship Program for financial aid. S.M. thanks the Canadian Government for their CRC Program.

References

[1] E. Larsson, J. Alegret, M. Käll, D. Sutherland, *Nano Letters* **2007**, *7*, 1256.

[2] S.M. Marinakos, S. Chen, A. Chilkoti, *Analytical Chemistry* **2007**, *79*, 5278.

[3] S.M.H. Rafsanjani, T. Cheng, S. Mittler, C. Rangan, *Journal of Applied Physics* **2010**, *107*, 094303.

[4] S. Lee, M. Yamada, M. Miyake, *Carbon* **2005**, *43*, 2654.

[5] S. Bhaviripudi, E. Mile, S. a Steiner, A.T. Zare, M.S. Dresselhaus, A.M. Belcher, J. Kong, *Journal of the American Chemical Society* **2007**, *129*, 1516.

[6] V. Idakiev, Z.-Y. Yuan, T. Tabakova, B.-L. Su, *Applied Catalysis A: General* **2005**, *281*, 149.

[7] J. Hu, T.W. Odom, C.M. Lieber, *Accounts of Chemical Research* **1999**, *32*, 435.

[8] N. Chandrasekharan, P.V.P. Kamat, *The Journal of Physical …* **2000**, *104*, 10851.

[9] J.H. Lee, J.H. Park, J.S. Kim, D.Y. Lee, K. Cho, *Organic Electronics* **2009**, *10*, 416.

[10] N. Sakai, Y. Fujiwara, Y. Takahashi, T. Tatsuma, *Chemphyschem : a European Journal of Chemical Physics and Physical Chemistry* **2009**, *10*, 766.

[11] T. Jensen, L. Kelly, A. Lazarides, G.C. Schatz, *Journal of Cluster Science* **1999**, *10*, 295.

[12] K.L. Kelly, E. Coronado, L.L.L. Zhao, G.C. Schatz, *The Journal of Physical Chemistry B* **2002**, *107*, 668.

[13] G. Schatz, *Spring* **2005**, *7*, 2032.

[14] P.K. Jain, K.S. Lee, I.H. El-Sayed, M. a El-Sayed, *The Journal of Physical Chemistry. B* **2006**, *110*, 7238.

[15] X. Huang, P.K. Jain, I.H. El-Sayed, M. a El-Sayed, *Nanomedicine (London, England)* **2007**, *2*, 681.

[16] A.B. Dahlin, B. Dielacher, P. Rajendran, K. Sugihara, T. Sannomiya, M. Zenobi-Wong, J. Vörös, *Analytical and Bioanalytical Chemistry* **2012**, *402*, 1773.

[17] M.-C. Daniel, D. Astruc, *Chemical Reviews* **2004**, *104*, 293.

[18] M.J. Hampden-Smith, T.T. Kodas, *Chemical Vapor Deposition* **1995**, *1*, 8.

[19] N. Kaiser, *Applied Optics* **2002**, *41*, 3053.

[20] K. Choy, *Progress in Materials Science* **2003**, *48*, 57.

[21] T. Kodas, M.J. Hampden-Smith, *The Chemistry of Metal CVD*, VCH**1994**.

[22] M. Endo, K. Takeuchi, S. Igarashi, *Journal of Physics and …* **1993**, *54*, 1841.

[23] H. Dai, A. Rinzler, P. Nikolaev, *Chemical Physics …* **1996**, *4*.

[24] F.N. Ishikawa, M. Curreli, C.A. Olson, H.-I. Liao, R. Sun, R.W. Roberts, R.J. Cote, M.E. Thompson, C. Zhou, *ACS Nano* **2010**, *4*, 6914.

[25] Z. Zhang, L. Zhang, S. Senz, M. Knez, *Chemical Vapor Deposition* **2011**, *17*, 149.

[26] R. Palgrave, I. Parkin, *Gold Bulletin* **2008**, 0.

[27] A.K.A. Aliganga, F. Xu, W. Knoll, S. Mittler, in *Proceedings of SPIE*, SPIE**2005**, 59690H.

[28] R.G. Palgrave, I.P. Parkin, *Journal of the American Chemical Society* **2006**, *128*, 1587.

[29] R.G. Palgrave, I.P. Parkin, *Chemistry of Materials* **2007**, *19*, 4639.

[30] D. Barreca, A. Gasparotto, C. Maccato, E. Tondello, *Nanotechnology* **2008**, *19*, 255602.

[31] R. Binions, C. Piccirillo, R.G. Palgrave, I.P. Parkin, *Chemical Vapor Deposition* **2008**, *14*, 33.

[32] M.E. a. Warwick, C.W. Dunnill, R. Binions, *Chemical Vapor Deposition* **2010**, *16*, 220.

[33] J. Käshammer, P. Wohlfart, J. Weiß, C. Winter, *Optical Materials* **1998**, *9*, 406.

[34] P. Wohlfart, J. Weiβ, C. Winter, *Thin Solid Films* **1999**, *340*, 274.

[35] R. Fischer, U. Weckenmann, *Journal De Physique. IV* **2001**, *11*, 1183.

[36] M. Zinke-Allmang, *Thin Solid Films* **1999**, *346*, 1.

[37] C. Winter, U. Weckenmann, R.A. Fischer, * J. Käshammer, V. Scheumann, S. Mittler, *Chemical Vapor Deposition* **2000**, *6*, 199.

[38] A. Rezaee, K.K.H. Wong, T. Manifar, S. Mittler, *Surface and Interface Analysis* **2009**, *41*, 615.

[39] A.K. a. Aliganga, I. Lieberwirth, G. Glasser, A.-S. Duwez, Y. Sun, S. Mittler, *Organic Electronics* **2007**, *8*, 161.

[40] D. Trovo, E. Ertorer, R. Huang, T. Cheng, C. Rangan, S. Mittler, in *Modern Aspects of Electrochemistry*, **2013**, 104.

[41] A. Ulman, *Chemical Reviews* **1996**, *96*, 1533.

[42] F. Schreiber, *Progress in Surface Science* **2000**, *65*, 151.

[43] D. Schwartz, *Annual Review of Physical Chemistry* **2001**, 107.

[44] J.C. Love, L. a Estroff, J.K. Kriebel, R.G. Nuzzo, G.M. Whitesides, *Self-assembled Monolayers of Thiolates on Metals as a Form of Nanotechnology.*, **2005**.

[45] P.M. Tiwari, K. Vig, V. a. Dennis, S.R. Singh, *Nanomaterials* **2011**, *1*, 31.

[46] H. Li, J. Zhang, X. Zhou, G. Lu, Z. Yin, G. Li, T. Wu, F. Boey, S.S. Venkatraman, H. Zhang, *Langmuir : the ACS Journal of Surfaces and Colloids* **2010**, *26*, 5603.

[47] C.-S. Chiu, H.-M. Lee, C.-T. Kuo, S. Gwo, *Applied Physics Letters* **2008**, *93*, 163106.

[48] J. Yang, T. Ichii, K. Murase, H. Sugimura, *Langmuir : the ACS Journal of Surfaces and Colloids* **2012**, *28*, 7579.

[49] M.J. Madou, *Fundamentals of Microfabrication: The Science of Miniaturization*, CRC Press **2002**.

[50] J. Spinke, M. Liley, H.-J. Guder, L. Angermaier, W. Knoll, *Langmuir* **1993**, *9*, 1821.

[51] J. Dostálek, C.J. Huang, W. Knoll, in *Surface Design: Applications in Bioscience and Nanotechnology*, Wiley-VCH Verlag GmbH & Co. KGaA **2009**, 29.

[52] C. Corti, R. Holliday, *Gold Science and Application*, CRC Press **2010.**

[53] A. O. Borissova, A. A. Korlyukov, M. Y. Antipin, K. A. Lyssenko**,** *The Journal of Physical Chemistry A, Letters* **2008**, *112*, 11519.

[54] S. Lahmar, J.Maruani, S. Wilson, G. Delgad0-Barrio (Eds), *Progress in Theoretical Chemistry an Physics, Topics in the Theory of Chemical and Physical Systems*, Springer, Dordrecht **2007**.

[55] M. Gudiksen, *JOURNAL-AMERICAN* **2000**, 8801.

[56] S. Zou, G. Schatz, in *Surface-Enhanced Raman Scattering* (Eds: K. Kneipp, M. Moskovits, H. Kneipp), Springer Berlin / Heidelberg **2006**, 67.

[57] F. Toderas, M. Baia, L. Baia, S. Astilean, *Nanotechnology* **2007**, *18*, 255702.

[58] M. Fan, G.F.S. Andrade, A.G. Brolo, *Analytica Chimica Acta* **2011**, *693*, 7.

[59] N. Strekal, S. Maskevich, *Reviews in Plasmonics 2010* **2012**, *2010*, 283.

[60] G. Moula, R. Rodriguez-Oliveros, P. Albella, J. a. Sanchez-Gil, R.F. Aroca, *Annalen Der Physik* **2012**, *524*, 697.

[61] H. Jiang, T. Li, E. Ertorer, J. Yang, J. Sabarinathan, S. Mittler, *Sensors and Actuators A: Physical* **2013**, *189*, 474.

[62] L. Zhao, D. Jiang, Y. Cai, X. Ji, R. Xie, W. Yang, *Nanoscale* **2012**, *4*, 5071.

[63] G.J. Nusz, S.M. Marinakos, A.C. Curry, A. Dahlin, F. Höök, A. Wax, A. Chilkoti, *Analytical Chemistry* **2008**, *80*, 984.

[64] M. Fan, M. Thompson, M. Andrade, *Analytical Chemistry* **2010**, *82*, 6350.

[65] P. Rooney, A. Rezaee, S. Xu, T. Manifar, A. Hassanzadeh, G. Podoprygorina, V. Böhmer, C. Rangan, S. Mittler, *Physical Review B* **2008**, *77*, 1.

[66] A. Rezaee, L.C. Pavelka, S. Mittler, *Nanoscale Research Letters* **2009**, *4*, 1319.

[67] A. Rezaee, A.K. a Aliganga, L.C. Pavelka, S. Mittler, *Physical Chemistry Chemical Physics : PCCP* **2010**, *12*, 4104.

[68] A. Rezaee, A. Aliganga, S. Mittler, *The Journal of Physical Chemistry C* **2009**, *113*, 15824.

[69] H. Schmidbaur, A. Shiotani, *Chemische Berichte* **1971**, *104*, 2821.

[70] Rasband W. S., *Http://rsbweb.nih.gov/ij/* **2008**.